J Mater Sci (2013) 48:7783–7790
DOI 10.1007/s10853-013-7463-x

POLYMER FIBERS

Catalytic graphitization and formation of macroporous-activated carbon nanofibers from salt-induced and H_2S-treated polyacrylonitrile

Yakup Aykut · Behnam Pourdeyhimi · Saad A. Khan

Received: 31 January 2013 / Accepted: 23 May 2013 / Published online: 31 May 2013

Abstract We present here a facile method to produce macroporous-activated carbon nanofibers (AMP-CNFs) by post-treating electrospun cobalt(II) chloride ($CoCl_2$) containing polyacrylonitrile (PAN/$CoCl_2$) nanofibers with hydrogen sulfide (H_2S) followed by carbonization. A range of techniques including scanning and transmission electron microscopy, FTIR and Raman spectroscopy is used to examine and characterize the process. Because of the phase behavior between carbon and cobalt, cobalt particles are formed in the nanofibers, some of which leave the fibers during the heat treatment process leading to macroporous fibrous structures. The number of the macroporous increase significantly with increasing $CoCl_2$ concentration in the precursor H_2S-treated PAN/$CoCl_2$ nanofibers. The cobalt phase in the fibers also leads to catalytic graphitization of the carbon nanofibers. The produced AMP-CNFs may be a promising candidates in many applications including anode layer in lithium ion batteries, air and liquid purifiers in filters, as well as in biomedical applications.

This article is an extended version of the study presented at the Fiber Society 2012 Fall Conference at Boston, MA, USA.

Y. Aykut (✉)
Department of Textile Engineering, Uludag University, Gorukle, 16059 Bursa, Turkey
e-mail: yakupaykut@gmail.com

B. Pourdeyhimi
Fiber and Polymer Science, Department of Textile Engineering, Chemistry and Science, North Carolina State University, Raleigh, NC 27695-8301, USA

S. A. Khan
Chemical and Biomolecular Engineering, North Carolina State University, Raleigh, NC 27695-7905, USA

Introduction

Nanotechnological developments in the past decades have helped to improve device performances by either enhancing material properties or developing new processing techniques. Synthesis of carbon-based materials at the nanoscale can increase device performance by several orders of magnitude. Nanostructured carbon-based materials have been produced in the form of nanoparticles (fullerenes: $C_{60–100}$), nanofilms (graphene and graphite layers), and one dimensional (1D) carbon nanotubes (CNTs) via a variety of nanoprocessing techniques [1–3].

Producing carbon-based materials with porous structures in the nanoscale can further enhance the final device performance because the significant increase in total specific surface area leads to better interactions with the targets (can be another material, ion, light, etc.). Porous-activated carbon-based materials have been used for a variety of applications including for anode layers in lithium ion batteries, removing pollutants from air, air filter in gas masks and respirators, distilled alcoholic beverage purification, and controlling overdoses in oral ingestion in biomedical applications, etc. [4–8].

Electrospinning is a powerful processing technique to produce 1D continuous polymer, ceramic, metal, and composite nanofibers [9–12]. With this technique, carbon nanofibers can also be produced by using a variety of polymer precursors including PAN, polybenzimidazole (PBI), polyvinylalcohol (PVA), polyimides (PIs), and their blends [13–17]. Typically, in this process as-spun precursor nanofibers are stabilized in an air atmosphere, followed by carbonization in an inert atmosphere. To produce porous carbon nanofibers via electrospinning, a deviation of this procedure is used. Recently, Liu et al. [18] produced

multiple tubular porous structure of carbon nanofibers via electrospinning from a polymer blend solution of PAN and polylactide (PLA). They eliminate PLA from the fibers during the stabilization and carbonization process to obtain porous carbon nanofibrous structure. In another study, porous carbon nanofibrous structure was prepared by Yang et al. [19] via preparation of electrospun porous poly(vinylidene fluoride) fibers from solutions in dimethylformamide, poly(ethylene oxide) (PEO) and water, and converting as-spun fibers into carbon structure by carbonization at high temperatures. Wu et al. [20] produced porous carbon nanofibers through electrospinning of iron acetate and PAN solution and subsequent catalytic carbonization of the fibers.

In this study, we produced AMP-CNFs with macroporous morphology and enhanced graphitic structure. The method schematically illustrated in Fig. 1 builds on our previous study in which we synthesized activated carbon nanofibers with random porous structure by using the same precursor (PAN/$CoCl_2$) nanofibers [21]. In this study, we use an additional yet simple step of treating the PAN/$CoCl_2$ precursor nanofibers with H_2S before thermal stabilization and carbonization steps. Interestingly, after the carbonization of H_2S-treated PAN/$CoCl_2$ nanofibers, regular macroporous carbon nanofibers with enhanced graphitic structures are obtained.

Experimental section

Chemicals

Polyacrylonitrile (PAN, molecular weight of $\sim$150000 g mol^{-1}, Scientific Polymer Product Inc., Ontario, NY, USA), *N*,*N*-dimethylformamide (DMF, 99.9 % purity, Fisher Scientific Inc.), and hydrogen sulfide (H_2S water solution, 0.4 g H_2S per 100 ml solution) were used as received without any purification.

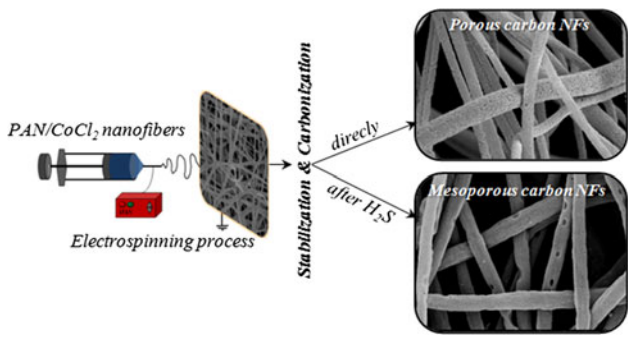

Fig. 1 Schematic illustration of the preparation mechanism of activated macroporous carbon nanofibers (AP-CNFs)

Electrospinning of $CoCl_2$-doped PAN nanofibers, and their treatment with H_2S and their further stabilization and carbonization

Electrospinning of $CoCl_2$-doped PAN nanofibers has been explained in detail in our previous article [21]. PAN and $CoCl_2$ dissolved in DMF and the prepared solution was electropun into nanofibrous structure. As-spun PAN/$CoCl_2$ nanofibers were soaked in H_2S (liquid) at room temperature for 1 h and then washed several times with distilled water and vacuum dried for 24 h. The dried nanofibers were then stabilized and carbonized in a Lindberg one-zone furnace within a quartz tube with inner diameter of 45 mm (Model 58114). The stabilization process was performed in air atmosphere (heated up to 280 °C with 5 °C min^{-1} heating rate and maintained for 1 h at that temperature to allow proper chemical reactions in the fibers) following which the carbonization process was conducted in a nitrogen atmosphere (heated up to 800 °C with 5 °C min^{-1} heating rate and maintained at that temperature for 2 h). Flow rate of the air and nitrogen gases during the heat treatment processes was very low.

Characterization of Nanofibers

Morphological characterizations of as-spun PAN/$CoCl_2$, H_2S-treaded PAN/$CoCl_2$, and carbonized macroporous carbon nanofibers were conducted with both transmission electron microscopy with acceleration voltage of 200 kV (TEM, Hitachi HF-2000) and scanning electron microscopy (SEM, FEI/Philips XL30 SEM-FEG, with an acceleration voltage of 5 kV, samples were coated with 100 Å thickness of gold before SEM analyses to reduce charging). Chemical analysis of the nanofibers was carried out with attenuated total reflection-Fourier transform infrared spectroscopy (ATR-FTIR, Thermo Scientific^{TM} FTIR with a Nexus 470 bench, wave number range of 4000–750 cm^{-1}, at least 124 scans were collected to minimize the noise, spectral resolution of 0.125 cm^{-1}) and a X-ray photoelectron spectroscopy (XPS, Kratos Analytical Axis Ultra XPS system), whereas thermal analysis of the nanofibers to screen the weight loss was performed in air and nitrogen atmospheres separately were done using thermo-gravimetric analysis (TA-Instruments TGA-Q500, heating from 25 to 800 °C, heating rate of 10 °C min^{-1}). Microstructures of macroporous carbon nanofibers were also examined using Raman spectra (Horiba Jobin–Yvon LabRAM ARAMIS microscope with the laser line at 632 nm, using He–Ne excitation source).

Results and discussions

Morphological features of the H_2S-treated pure PAN and PAN/$CoCl_2$ NFs obtained using SEM are shown in Fig. 2.

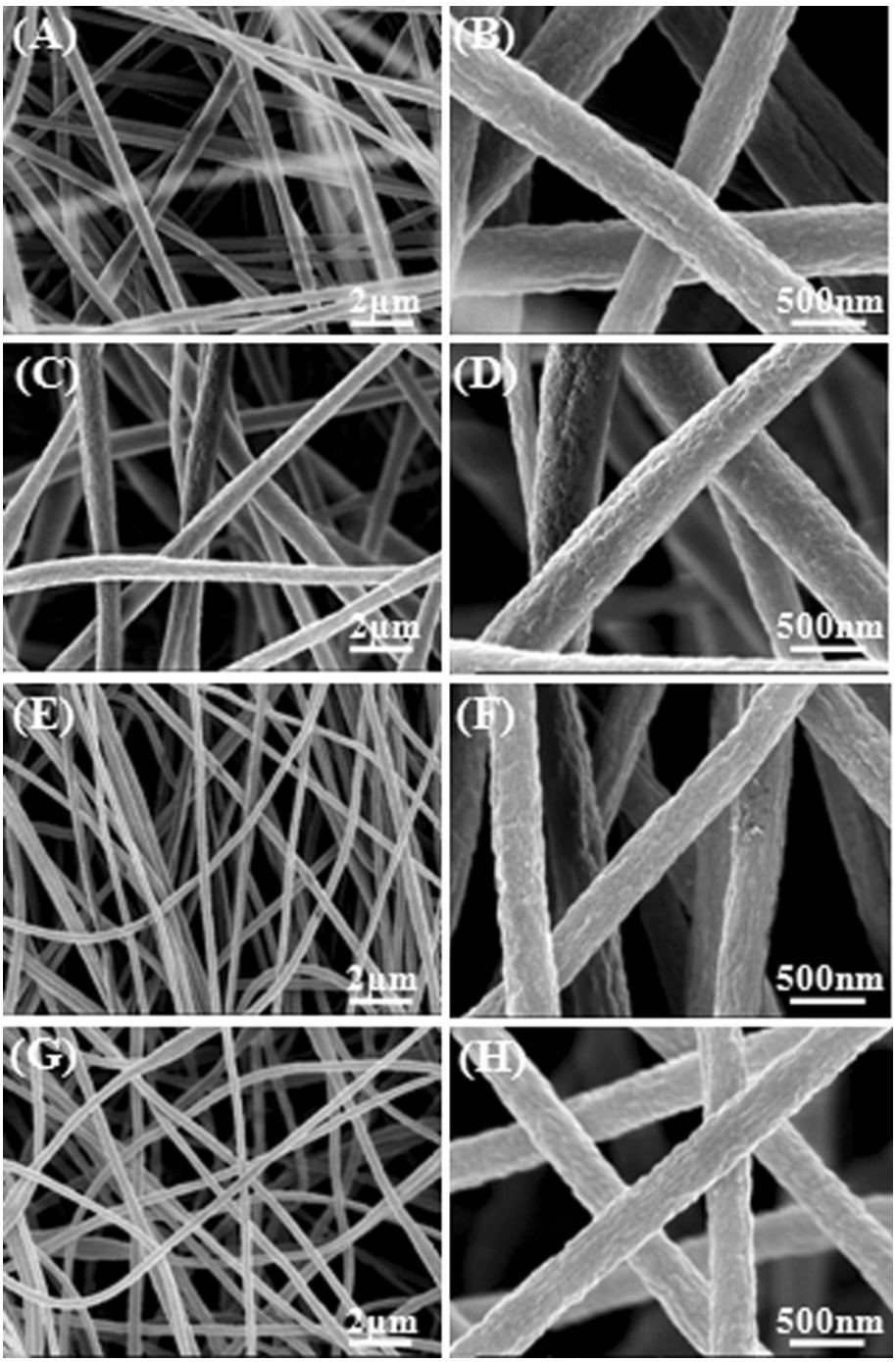

Fig. 2 SEM images of electrospun H_2S-treated PAN–$CoCl_2$ precursor composite nanofibers with different $CoCl_2$ contents (wt%): **a**, **b** 0 (pure CNFs); **c**, **d** 1; **e**, **f** 5; and **g**, **h** 30

We find all nanofibers to be relatively uniform, randomly oriented, and forming a 3D interwoven network structure. The differences among the nanofibers in Fig. 2 can be clearly seen in the TEM images and explained at TEM imaging section. The ATR-FTIR of pure PAN, PAN/$CoCl_2$, and H_2S-treated PAN/$CoCl_2$ composite nanofibers were recorded in the 750–3550 cm^{-1} wavelength range and shown in Fig. 3A. The characteristic peaks of PAN observed at ca. 2921 and 2242 cm^{-1} are assigned to methylene (CH_2) and nitrile ($C\equiv N$) stretching vibrations, respectively [22]. Bending and stretching vibrations of CH_2 groups are seen at ca. 1452 and 2921 cm^{-1} [21, 23]. Stretching and bending vibration peaks of the hydroxyl (OH) groups that come from the adsorbed water are seen at ca. 3631 and 1664 cm^{-1}, respectively, [24, 25]. The intensities of these peaks increase and get broader with $CoCl_2$ content in as-spun PAN/$CoCl_2$ NFs (Fig. 3A, a), and then decrease again after H_2S treatment as a result of drying in vacuum (Fig. 3A, b). The dried H_2S-treated PAN/$CoCl_2$ NFs were also analyzed with XPS to examine the

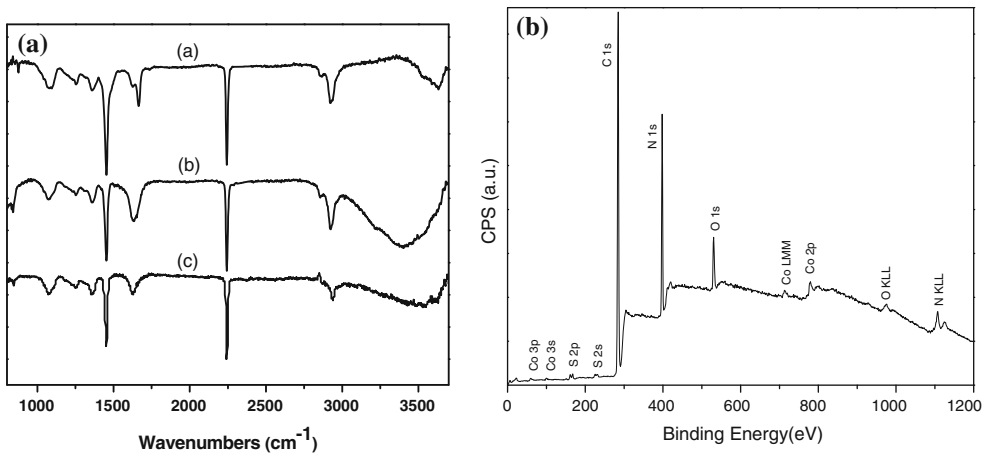

Fig. 3 **a** The attenuated total reflection-Fourier transform infrared spectra (ATR-FTIR) of *a* pure PAN, *b* PAN/$CoCl_2$, and *c* H_2S-treated PAN/$CoCl_2$ composite nanofibers. **b** X-ray photoelectron spectra (XPS) of H_2S-treated PAN/$CoCl_2$ composite nanofibers

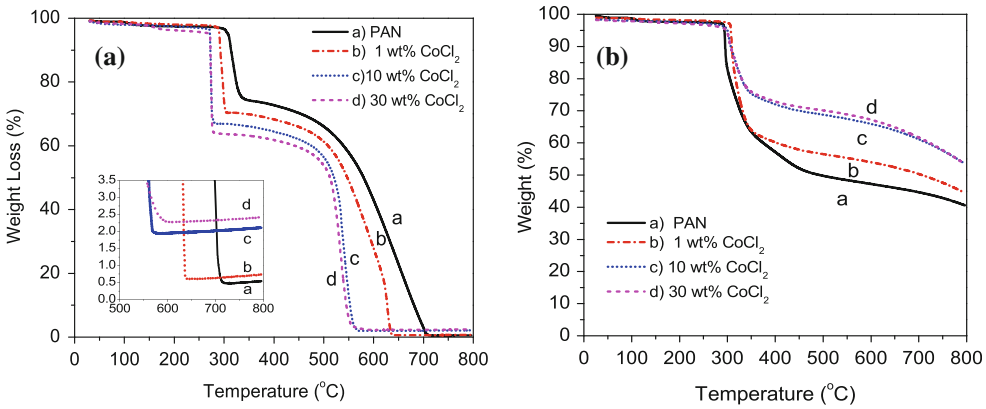

Fig. 4 Thermal-gravimetric-analysis (TGA) of electrospun H_2S-treated PAN/$CoCl_2$ composite nanofibers with different $CoCl_2$ contents (wt%): *a* 0 (pure PAN), *b* 1, *c* 10, and *d* 30 (**a**) in air atmosphere and **b** in nitrogen atmosphere

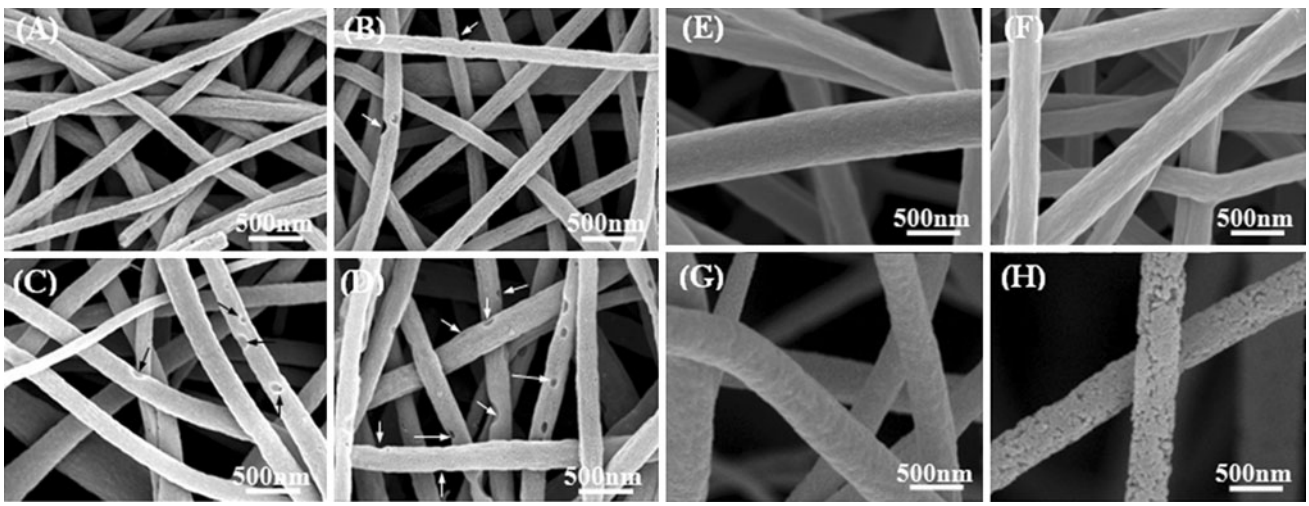

Fig. 5 SEM images of electrospun AMP-CNFs with different $CoCl_2$ contents (wt%) in the H_2S-treated $CoCl_2$/PAN precursor composites: **a** 0 (pure CNFs), **b** 1, **c** 5, and **d** 30. SEM images of these carbonized nanofibers without H_2S-treated $CoCl_2$/PAN precursor composites: **e** 0 (pure CNFs), **f** 1, **g** 5, and **h** 30

elemental composition of the NFs (Fig. 3B). All peaks representative of the formation of cobalt sulfide is observed on the fibers after H_2S treatment.

Thermogravimetric measurements in air (Fig. 4A) and nitrogen (Fig. 4B) atmospheres were conducted to screen weight loss and heat of reactions of H_2S-treated pure PAN and PAN/$CoCl_2$ NFs during the stabilization and carbonization processes. As seen from Fig. 4, weight loss primarily takes place in two steps, at 300 °C (cyclization and removal of volatiles) and at 500 °C (compositional removal of the byproducts) when we heat the samples in air atmosphere [26, 27]. When we increase the content of $CoCl_2$ in the as-spun PAN/$CoCl_2$ NFs and treat them with H_2S under the same conditions, these two temperatures decreases consistently. The presence of $CoCl_2$ initiates the reactions in PAN NFs so the weight loss starts at a lower temperature and this temperature decreases with increasing $CoCl_2$ contents in the fibers. Meanwhile, the residues of the H_2S-treated PAN/$CoCl_2$ NFs at 800 °C increase (0.53, 0.71, 2.11, and 2.41 %, respectively, for 0, 1, 5, and

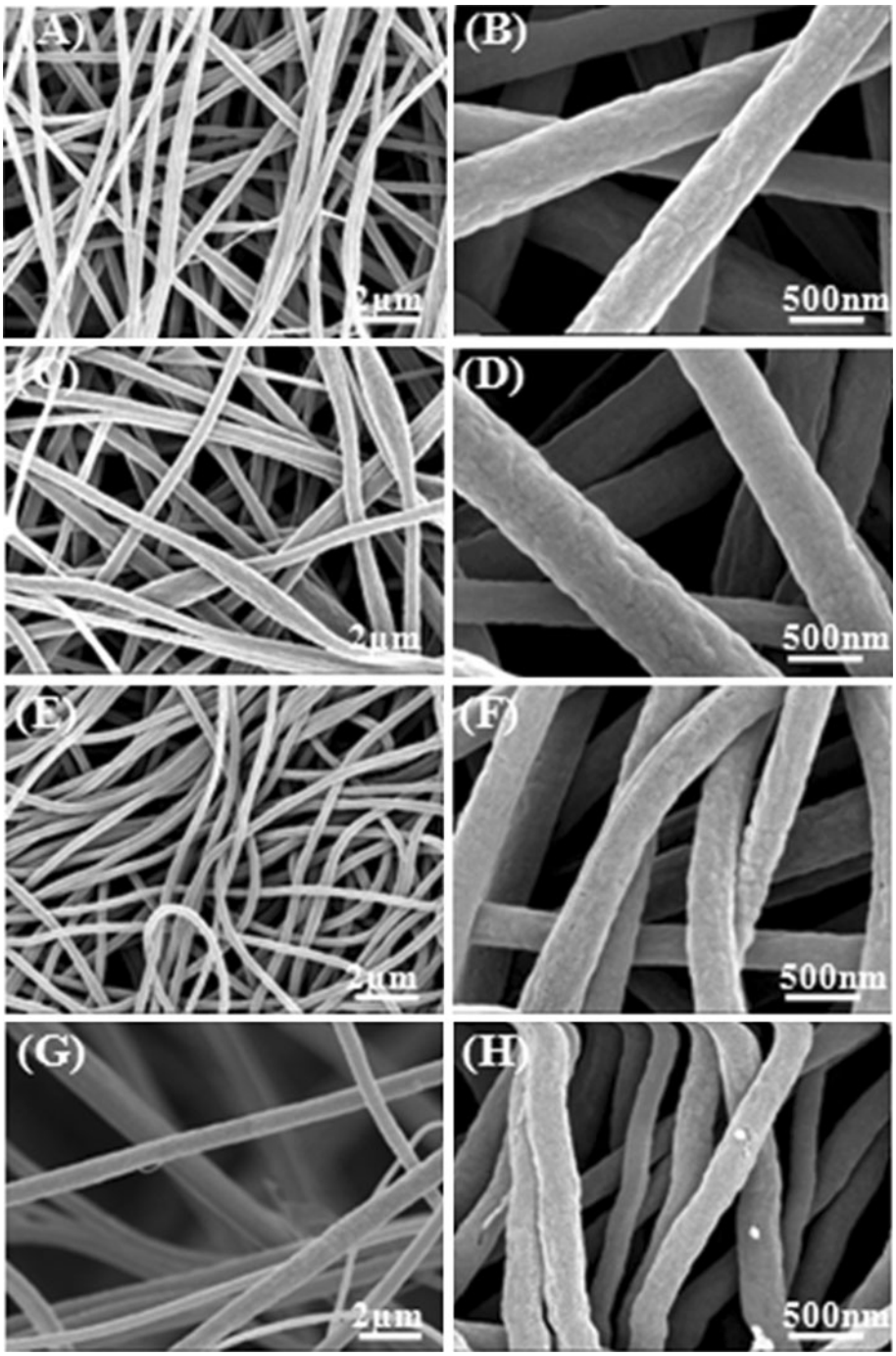

Fig. 6 SEM images of the stabilized electrospun the H_2S-treated $CoCl_2$/PAN precursor composite nanofibers with different $CoCl_2$ contents (wt%): **a**, **b** 0 (pure CNFs); **c**, **d** 1; **e**, **f** 5; and **g**, **h** 30

30 wt% H_2S-treated PAN/$CoCl_2$ NFs) because of the existence of cobaltous phase and oxidation of some of them.

A TGA plot of H_2S-treated PAN/$CoCl_2$ NFs under a nitrogen environment is shown in Fig. 4B. We observe a sharp decrease in weight around 280–300 °C, followed by a slow decay as the temperature is increased. The sharp weight loss can be attributed to removal of volatiles and the complex chemical reactions that occur during the stabilization process (dehydrogenation, cyclization, and crosslinking) [26, 27]. The residuals at 800 °C are also consistently increasing (40.61, 44.51, 53.58, and 53.45 %, respectively, for 0, 1, 5, and 30 wt% H_2S-treated PAN/$CoCl_2$ NFs) with increasing $CoCl_2$ content in H_2S-treated NFs and corresponds to macroporous carbon nanofibers.

SEM images of the carbonized pure PAN and H_2S-treated PAN/$CoCl_2$ NFs are shown in Fig. 5. We find that the carbonized fibers obtained from PAN (CNF) to be uniform and showing no porosity (Fig. 5a). However, macroporous structures are seen after carbonization of the H_2S-treated PAN/$CoCl_2$ composite NFs, with the number of the pores increasing with increasing $CoCl_2$ content in the precursor H_2S-treated PAN/$CoCl_2$ NFs (Fig. 5b–d). The formation of macroporous structure can be explained by the activation of carbon nanofibers and the migration of cobaltous phase in the fibers during the heat treatment processes. Macroporous structure is obtained (average pore diameter of around 71 nm) because the particles move and escape from the fibers. The motion of cobalt particles in carbon nanofibers can be explained by the phase behavior of cobalt and carbon at high temperatures. In our study, we envisage cobalt particles migrate in the fibers, come together to form big particles, and then dislodge from the fibers. As a result, both the number of the pores and the average diameters of the AMP-CNFs increase with increasing $CoCl_2$ in the precursor H_2S-treated PAN/$CoCl_2$ NFs. Random pore formation in the carbonized nanofibers without H_2S-treated $CoCl_2$/PAN precursor composites was reported in our previous study shown in Fig. 5e–h for comparison. Interestingly, average fiber diameter decreases dramatically after carbonization comparing H_2S-treated and -untreated nanofibers. This can be attributed to removal of vast amount of cobaltous phase from the fibers after carbonization of H_2S-treated CNFs. The evidence of this can be found from the TEM imaging.

To further understand the phenomenon, SEM images of stabilized H_2S-treated PAN/$CoCl_2$ composite nanofibers at 280 °C in air are taken and shown in Fig. 6a–h. Because of complex chemical reactions (dehydrogenation, cyclization, and crosslinking) during the stabilization process fibers

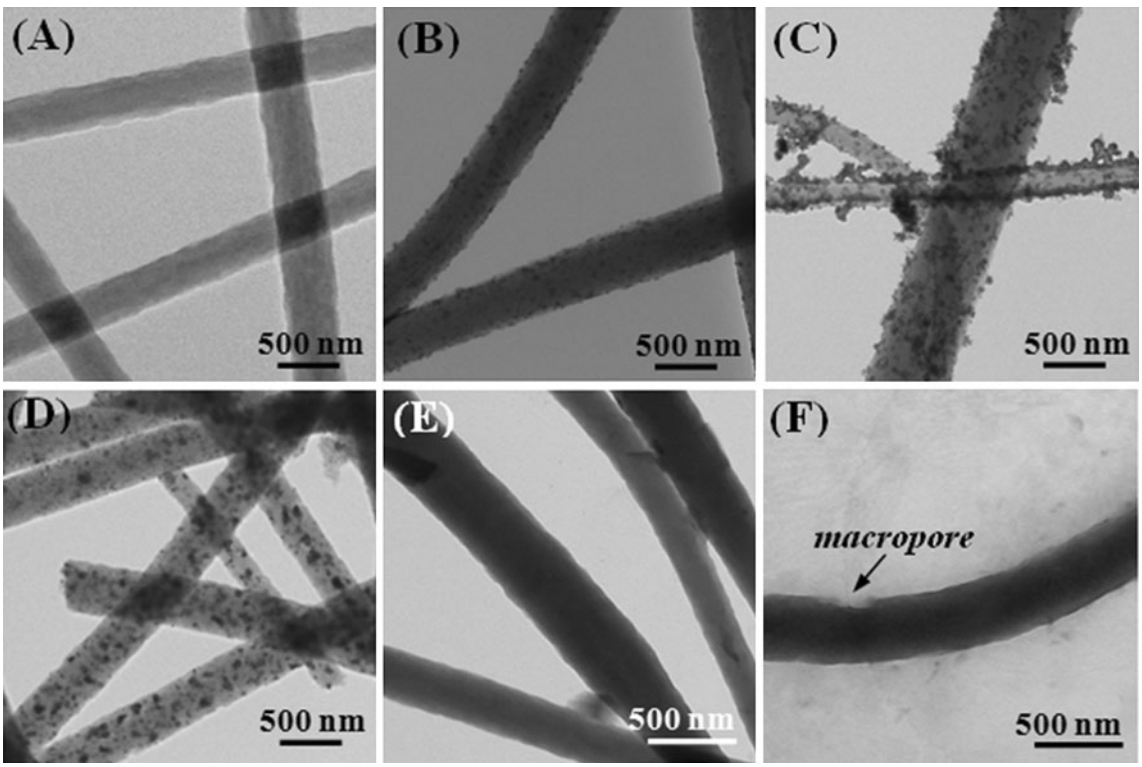

Fig. 7 TEM images of the nanofibers: **a** PAN, **b** PAN/$CoCl_2$, **c** H_2S-treated PAN/$CoCl_2$, **d** CNFs of the $CoCl_2$/PAN precursor composites nanofibers, and **e**, **f** AMP-CNFs of the H_2S-treated $CoCl_2$/PAN precursor composites nanofibers. The content of $CoCl_2$ in the nanofibers is 30 wt%

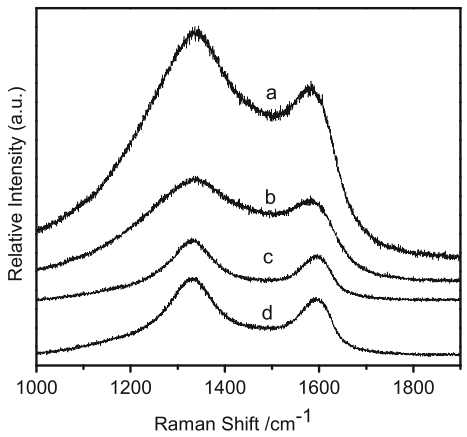

Fig. 8 Raman spectra of AMP-CNFs with different $CoCl_2$ contents in the precursor H_2S-treated $CoCl_2$/PAN composites: **a** 0 (pure CNFs), **b** 1, **c** 5, and **d** 30 wt%

Table 1 Raman spectra intensities of AMP-CNFs with different $CoCl_2$ contents in the precursor H_2S-treated $CoCl_2$/PAN composites

$CoCl_2$ content (wt%)	0 (wt%)	1 (wt%)	5 (wt%)	30 (wt%)
1329 cm^{-1} (D-band)	1343	1333	1329	1323
1571 cm^{-1} (G-band)	1570	1582	1596	1594
$R = (I_D/I_G)$	0.855	0.842	0.832	0.829

Raman spectra (Horiba Jobin–Yvon LabRAM ARAMIS microscope with the laser line at 632 nm, using He–Ne excitation source)

swell, average nanofiber diameter increases tremendously and surface of the fibers becomes much smoother in comparison with as-spun nanofibers.

To understand macroporous formation, TEM images of pure PAN, PAN/$CoCl_2$, H_2S-treated PAN/$CoCl_2$, and AMP-CNFs of the H_2S-treated $CoCl_2$/PAN precursor nanofibers were obtained and shown in Fig. 7. As-spun PAN NFs are almost translucent (Fig. 7a) and $CoCl_2$ nanoparticles are evident in PAN/$CoCl_2$ NFs corresponding to the dark regions in Fig. 7b. Fuzzy surface represents the formation of cobalt sulfide after soaking as-spun PAN/$CoCl_2$ NFs in H_2S (Fig. 7c). During the stabilization and carbonization process, the cobalt phases migrate and escape from the NFs, leaving macroporous structures behind them (Fig. 7e–f). CNF without H_2S processing shows dark domains correspond to cobalt particles (Fig. 7d), but these domains cannot be seen at H_2S-treated CNFs (Fig. 7e–f).

In order to determine the graphitic structures of the carbonized NFs, Raman spectra of the NFs were conducted and are shown in Fig. 8 and Table 1. We observe two distinct peaks at ca. 1329 cm^{-1} (D-band) and 1571 cm^{-1} (G-band) that can be attributed to the carbon structure; these peaks correspond to the disordered carbons in graphene layers and ordered graphite phases in the AMP-CNFs [21, 28]. The intensity ratios $R = (I_D/I_G)$ of these peaks indicate the nature of the structural order of the graphitic phase in the CNFs. The R value decreases slightly with increasing $CoCl_2$ content in the precursor H_2S-treated $CoCl_2$/PAN (Fig. 8a–d) [28]. The decrease of this ratio for macroporous CNFs indicates that more ordered graphitic structures are obtained with the presence of cobalt phase because of the catalytic graphitization of the nanofibers.

Conclusions

AMP-CNFs were synthesized by post treatment of electrospun PAN/$CoCl_2$ composite NFs with H_2S followed by stabilization and carbonization. Because of the different phase behavior of cobalt and carbon, AMP-CNFs structures are obtained after the heat treatment processes. The number of the macroporous dramatically increases when we increase the $CoCl_2$ contents in the precursor H_2S-treated PAN/$CoCl_2$ nanofibers. The results reveal that graphitic structure of macroporous CNFs is obtained because cobalt in the fibers promotes catalytic graphitization during the carbonization process.

Acknowledgements The authors acknowledge funding support from the Nonwovens Cooperative Research Center, NCRC at North Carolina State University and the Ministry of National Education of the Republic of Turkey. YA thanks Dr. Dale Bachelor at the Analytical Instrumentation Facility, NCSU for his assistance in TEM sample characterization.

References

1. Dresselhaus MS, Dresselhaus G, Eklund PC (1996) Science of fullerenes and carbon nanotubes. Academic Press, New York
2. Vaughan O (2010) Nat Nanotechnol 5:386
3. Baddour CE, Fadlallah F, Nasuhoglu D, Mitra R, Vandsburger L, Meunier JL (2009) Carbon 47:313
4. Ji L, Zhang X (2009) Electrochem Commun 11:684
5. Wang Z, Zhang JS (2011) Build Environ 46(758):768
6. Romero JV, Smith JWH, Sullivan BM, Mallay MG, Croll LM, Reynolds JA, Andress C, Simon M, Dahn JR (2011) ACS Comb Sci 13:639
7. Soto ML, Moure A, Dominguez H, Parajo JC (2011) J Food Eng 105:1
8. Eyer F, Jung N, Neuberger N, Witte A, Poethko T, Henke J, Zilker T (2008) Basic Clin Pharmacol 102:337
9. Huang ZM, Zhang YZ, Kotaki M, Ramakrishna S (2003) Compos Sci Technol 63:2223
10. Li D, Xia Y (2004) Adv Mater 16(14):1151
11. Wu H, Hu L, Rowell MW, Kong D, Cha JJ, McDonough JR, Zhu J, Yang Y, McGehee MD, Cui Y (2010) Nano Lett 10:4242
12. Sahay R, Kumar PS, Sridhar R, Sundaramurthy J, Venugopal J, Mhaisalkar SG, Ramakrishna S (2012) J Mater Chem 22:12953
13. Yan KS, Kim C, Park SH, Kim JH, Lee WJ (2006) J Biomed Nanotechnol 2:103
14. Fatema UK, Uddin AJ, Uemura K, Gotoh Y (2011) Text Res J 81:659

15. Chung GS, Jo SM, Kim BC (2005) J Appl Polym Sci 97:165
16. Kim C, Park SH, Lee WJ, Yang KS (2004) Electrochim Acta 50:877
17. Kim C, Cho YJ, Yun WY, Ngoc BTN, Yang KS, Chang DR, Lee JW, Kojima M, Kim YA, Endo M (2007) Solid State Commun 142:20
18. Liu T, Gu SY, Zhang YH, Ren J (2012) J Poly Res 19:9882
19. Yang Y, Centrone A, Simeon F, Hatton TA, Rutledge GC (2011) Carbon 49:3395
20. Wu J, Park HW, Yu A, Higgins D, Chen Z (2012) J Phys Chem 116:9427
21. Aykut Y (2012) Appl Mater Interfaces 4:3405
22. Ko TH, Chen CY (1999) J Appl Polym Sci 74:1745
23. Kang YH, Ahn K, Jeong SY, Bae JS, Jin JS, Kim HG, Hong SW, Cho CR (2011) Thin Solid Films 519:7090
24. Deng S, Bai R, Chen JP (2003) J Colloid Interface Sci 260:265
25. Rahman MM, Jamal A, Khan SB, Faisal M (2011) J Phys Chem 115:9503
26. Chen IH, Wang CC, Chen CY (2010) Carbon 48:604
27. Ji L, Medford AJ, Zhang X (2009) J Mater Chem 19:5593
28. Kim C, Yang KS, Kojima M, Yoshida K, Kim YJ, Kim YA, Endo M (2006) Adv Funct Mater 16:2393